ACS OMEGA

http://pubs.acs.org/journal/acsodf

Article

Effects of MXene on Nonisothermal Crystallization Kinetics of Isotactic Polypropylene

Wanxin Peng, Ran Hu, Weijiao Jiang, Jian Kang,* Jingping Li,* Ya Cao, and Ming Xiang

Cite This: *ACS Omega* 2021, 6, 19973−19982

Read Online

ACCESS | Metrics & More | Article Recommendations

ABSTRACT: MXenes, a family of two-dimensional transition-metal carbides/nitrides, have attracted great attention and shown promising application in polymer composites. In this study, a typical MXene $Ti_3C_2T_x$ was prepared by selective etching. The structure and morphology of $Ti_3C_2T_x$ were studied by X-ray diffraction (XRD), scanning electron microscopy, and transmission electron microscopy, and the results proved that $Ti_3C_2T_x$ was successively fabricated. Then, $Ti_3C_2T_x$/isotactic polypropylene composites with different $Ti_3C_2T_x$ dosages were fabricated, and the nonisothermal crystallization kinetics and melting behavior of the composites were investigated. The results indicated that when a small amount of $Ti_3C_2T_x$ was added, the crystallization parameters including the crystallization peak temperature and the crystallization rate increased, suggesting that crystallization was promoted. When the weight percentage of $Ti_3C_2T_x$ exceeded 1%, the crystallization parameters showed a reverse trend, suggesting that crystallization was hindered. The activation energy of composites with 0, 0.25, 0.5, and 1 wt % $Ti_3C_2T_x$ were calculated to be −164.5, −196.5, −193.8, and −147.95 kJ/mol, respectively, revealing that the crystallization of composites is concentration-dependent. The impact of $Ti_3C_2T_x$ dosage on the crystalline structure of the composites was studied using XRD. The related mechanism was proposed.

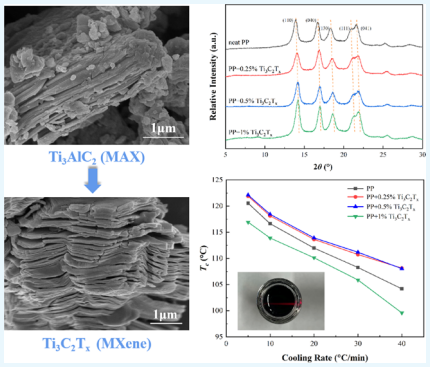

1. INTRODUCTION

In the past decade, two-dimensional (2D) materials have attracted significant attention and have been widely researched since single-layer graphene was exfoliated from graphite by the team of Novoselov and Geim in 2004.[1] Due to their unique structure, 2D materials often possess superior physical, electronic, optical, and mechanical properties, leading to great potential application in many fields including energy storage, supercapacitor, composites, *etc.* Apart from graphene, many types of 2D materials such as metal−organic frameworks (MOFs),[2,3] covalent−organic frameworks (COFs),[4,5] and black phosphorus (BP)[5] have been studied.[6] In 2011, Gogotsi, Barsoum, and their team discovered and synthesized 2D transitional-metal carbides for the first time, which are called MXene.[7]

MXenes are a family of transition-metal carbides/nitrides with a general chemical formula $M_{n+1}X_nT_x$ (n = 1, 2, 3), where M stands for an early transition metal, X stands for C/N, and T_x stands for possible surface terminations such as F^-, O^-, Cl^-, and OH^-. They are derived from MAX phases (A is usually elements from groups 12−16, such as Cd, Al, Si, P, S, Ga, Ge, As, In, Sn, Tl, Pb, and S[8]), which have a layered hexagonal structure with two formula units per unit cell.[2] Because A layer is relatively weakly bonded, the A layer atoms can be removed by selective etching. Since 2011, researchers have widely studied and synthesized about 30 different MXenes to explore their properties.[9] Among the MXenes materials, titanium carbide (Ti_3C_2) is one of the most promising and widely studied[10] and is usually synthesized by etching from its MAX phase Ti_3AlC_2. Like other 2D materials, MXenes have excellent properties due to their interesting structure and high surface area and therefore exhibit promising application in the fields of polymers. Many studies have been conducted to synthesize MXene-polymer composites. Zheng et al. produced Ti_3C_2/ultrahigh-molecular-weight polyethylene (UHMWPE) composites by the hot-pressing method.[11] The results indicate that Ti_3C_2/UHMWPE composites exhibit improved mechanical properties and decreased antifriction performance. Woo et al. fabricated functionalized MXene (f-MXene)/boric acid (BA)/poly(vinyl alcohol) (PVA) composites, which show enhanced thermal stability and mechanical and oxygen gas barrier properties, making MXene/BA/PVA composite a potential gas barrier film.[12] Liu et al. fabricated $Ti_3C_2T_x$-rGO/thermoplastic polyurethane elastomer (TPU) composites via the solvent-mixing melt blending method, and the results indicated that the peak smoke production rate and the total smoke release

Received: June 6, 2021
Accepted: July 14, 2021
Published: July 22, 2021

were remarkably decreased by 81.2 and 54%, respectively, with the addition of 2 wt % $Ti_3C_2T_x$-rGO.[13] Shi et al. prepared multifunctional nanohybrid $Ti_3C_2T_x$ with melamine cyanurate (MCA) to fabricate $Ti_3C_2T_x$@MCA/TPU nanocomposites and found that the nanocomposites show improved mechanical properties including high tensile strength of 61.5 MPa, high strain at failure of 588.4%, and remarkably high toughness of 175.4 MJ m^{-3}.[14]

Isotactic polypropylene (PP), one of the most commonly used conventional thermoplastic materials, has been widely used in fields such as automobile, packaging, and electronic devices due to its low manufacturing cost, ease of processing, and other excellent properties such as high toughness, elasticity, transparency, and impermeability.[15−17] However, mechanical properties such as weak impact strength and undesired thermal properties limit the application of polypropylene in some high-technology fields. Over the past few decades, incorporating inorganic fillers into a polymer matrix has become a widespread method to improve its physical properties.[18] It has been found that nanoparticles such as graphene oxide (GO),[19] surface-modified carbon black (CB),[20] silicon dioxide (SiO_2),[21] *etc.*, can improve the mechanical properties of polypropylene while promoting crystallization by functioning as nucleating agents. Since $Ti_3C_2T_x$ has a similar structure to graphene oxide, it can be considered as a potential nanofiller to PP. Inspired by the nanoconfinement structure, Shi et al. fabricated a $Ti_3C_2T_x$/PP nanocomposite with improved mechanical and thermal properties by the melt blending methods. It was discovered that the strength, ductility, and modulus were simultaneously enhanced by adding 2 wt % $Ti_3C_2T_x$.[22]

While current studies on the $Ti_3C_2T_x$/PP nanocomposite mainly focus on the change in thermal and mechanical properties, the crystallization process is not investigated in depth. It is known that the crystallization behavior of crystalline polymers can affect the physical and mechanical properties, therefore understanding the crystallization kinetics is of great importance. In this work, $Ti_3C_2T_x$/PP composites with different weight fractions were fabricated, followed by the analysis of the nonisothermal crystallization kinetics and melting behavior.

2. RESULTS AND DISCUSSION

2.1. Structure and Morphology of $Ti_3C_2T_x$. To check the structure and morphology of the $Ti_3C_2T_x$ powder, XRD, SEM, and TEM were conducted. As shown in Figure 1, the peaks of precursor Ti_3AlC_2 diminish gradually after etching. It is worth noting that the strongest (104) peak of Ti_3AlC_2 at $2\theta \approx 38.9°$ disappears, indicating the removal of the Al layer and thus the transformation from Ti_3AlC_2 to $Ti_3C_2T_x$.[23] It is worth noting that the (002) peak at around 9.6° shifts to 6.4° after etching, which is caused by the increase in the interlayer distance. Moreover, the broadening of the (002) peak after etching may be attributed to the decrease in the structural order.[24]

The morphology and chemical composition can be investigated by SEM and EDS. Figure 2a indicates that Ti_3AlC_2 powders exhibit a compact layered morphology that is often observed in ternary carbide.[25] Figure 2b exhibits an accordion-like multilayer structure of $Ti_3C_2T_x$ after etching, which is caused by exfoliation of the Al layer and suggests the success of the etching process.[8,26] Moreover, it is observed that the layer structure expanded compared with the structure of

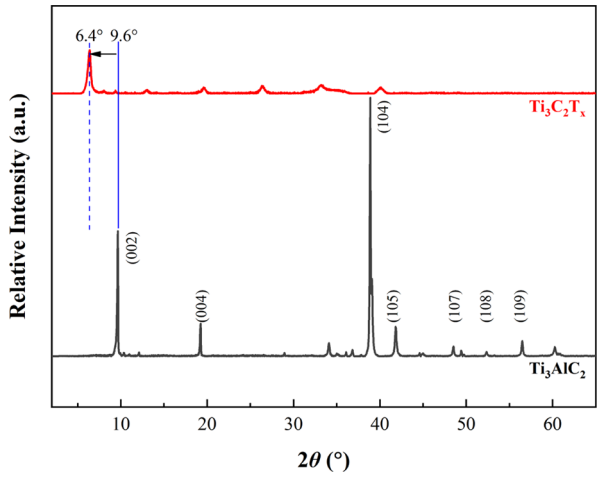

Figure 1. XRD curves of Ti_3AlC_2 and $Ti_3C_2T_x$ particles.

original Ti_3AlC_2, which is possibly caused by the gas escaping during (i.e., H_2) due to the exothermic nature of the reaction between HF and Al.[25] From the EDS results, the $Ti_3C_2T_x$ sample consists of Ti, C, O, F, and Al elements in the atomic ratio 21.9:28.3:27.7:20.5:1.6. During the etching process, two solid products may exist in the solution according to the equation

$$Ti_3AlC_2(s) + 3HF(l) \rightarrow Ti_3C_2(s) + AlF_3(s) + (3/2)H_2(g) \quad (1)$$

The presence of the Al element suggests the existence of AlF_3 impurities,[27] which form small balls attached to the surface of $Ti_3C_2T_x$.

Figure 3 shows that the diluted $Ti_3C_2T_x$ dispersion has a light green color and shows the Tyndall scattering effect. From the TEM image (Figure 4), it can be observed that $Ti_3C_2T_x$ has a sheet-like morphology, which is ultrathin and has a lateral size of a few hundred nanometers. Together with XRD, SEM, and EDS results, it can be concluded that $Ti_3C_2T_x$ was successively synthesized by etching.

2.2. Nonisothermal Crystallization Kinetics of the Composites. In the following section, the investigation of the crystallization kinetics is performed on the PP/$Ti_3C_2T_x$ composites. Figure 5 displays the cooling curve of each sample under cooling rates of 5, 10, 20, 30, and 40 °C/min. It can be seen that the cooling curves of the four samples have a similar variation tendency: as the cooling rate increases, the crystallization peak shifts toward lower temperature and becomes broader. Furthermore, the crystallization peak width (i.e., the difference between the onset and endpoint temperatures of crystallization, $T_{conset}-T_{cendpoint}$), as well as the crystallization peak temperature T_c, was calculated as indicators of the impact of $Ti_3C_2T_x$ on the crystallization of the composites. Figure 6 shows T_c and $T_{conset}-T_{cendpoint}$ as a function of the cooling rate of four samples. For all samples, T_c and $T_{conset}-T_{cendpoint}$ both increase with a higher cooling rate. At higher cooling rates, PP chains have limited time to move and rearrange in order; therefore, the crystallization process requires a larger extent of supercooling.

The addition of $Ti_3C_2T_x$ altered the crystallization behavior; when the weight percentage of $Ti_3C_2T_x$ increases from 0 to 0.25 and 0.5%, the values of both crystallization peak temperature and crystallization peak width increase. When

https://doi.org/10.1021/acsomega.1c02970
ACS Omega 2021, 6, 19973−19982

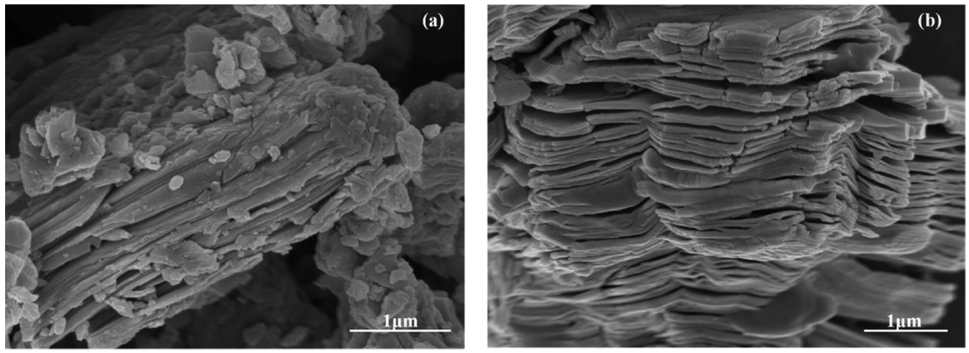

Figure 2. SEM images of (a) Ti_3AlC_2 and (b) $Ti_3C_2T_x$ particles. The precursor Ti_3AlC_2 has a condensed layer structure. $Ti_3C_2T_x$ also has a multilayer structure, and the space between layers expands.

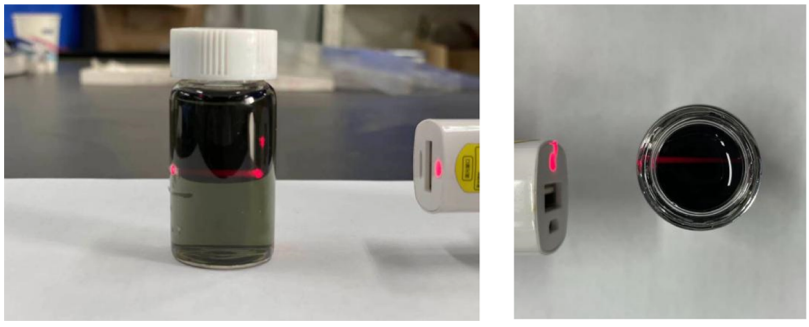

Figure 3. Digital photos of Ti_3C_2 dispersion.

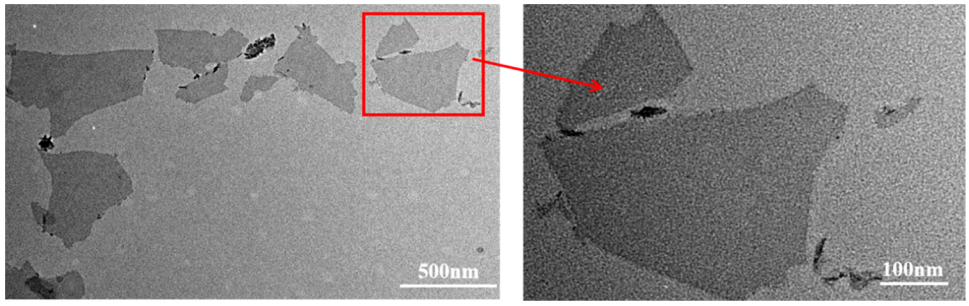

Figure 4. TEM image of Ti_3C_2 dispersion.

the weight percentage of $Ti_3C_2T_x$ further increases to 1%, the crystallization peak temperature drops to a value lower than of neat PP. The crystallization peak width first declines with the addition of more $Ti_3C_2T_x$ then starts to grow when the weight fraction of $Ti_3C_2T_x$ is 1 wt %. At a higher cooling rate (30 and 40 °C/min), the crystallization peak width of 1 wt % $Ti_3C_2T_x$ is the highest. A possible explanation has been proposed here. To the best of our knowledge, the crystallization theory divides crystallization into two processes: nucleation and growth. For neat PP, the crystallization nucleation is homogeneous. When $Ti_3C_2T_x$ are added to the PP matrix, they might tend to be adsorbed on the polymer chains due to their highly active surface and therefore act as heterogeneous nucleation sites.[11,28] In other words, the introduction of $Ti_3C_2T_x$ might provide more nucleation sites and then promote the crystallization process. The more the nucleation sites, the better the ability of the polymer to crystallize. As a result, the crystallization parameters including the crystallization peak temperature shift to higher values. In addition, polypropylene contains chains with different crystallization abilities. When the crystallization process is promoted, more PP chains can participate in crystallization. On the one hand, the part of chains with stronger crystallization ability becomes more easily crystallize, so T_{conset} shifts to a higher temperature. On the other hand, the part of chains that cannot crystallize before can now crystallize but requires a larger extent of overcooling; therefore, $T_{cendpoint}$ may shift to a lower temperature. As a result, the crystallization peak width may become wider.

The cumulative relative crystallinity vs crystallization time curve is shown in Figure 7. It is obvious to see that the addition of $Ti_3C_2T_x$ leads to a decrease in the crystallization time. To further analyze the crystallization behavior, half-crystallization time $t_{1/2}$ (i.e., the time when relative crystallinity reaches 50%) can be calculated. Table 1 reveals that at a lower cooling rate, the value of $t_{1/2}$ decreases continuously with the addition $Ti_3C_2T_x$ but increases again when the weight fraction of $Ti_3C_2T_x$ reaches 1%. At a higher cooling rate, $t_{1/2}$ of PP + 0.25% $Ti_3C_2T_x$ is smaller than those of others. It can be concluded that the crystallization rate tends to first increase and then decrease as more $Ti_3C_2T_x$ is added to the polymer matrix.

https://doi.org/10.1021/acsomega.1c02970
ACS Omega 2021, 6, 19973−19982

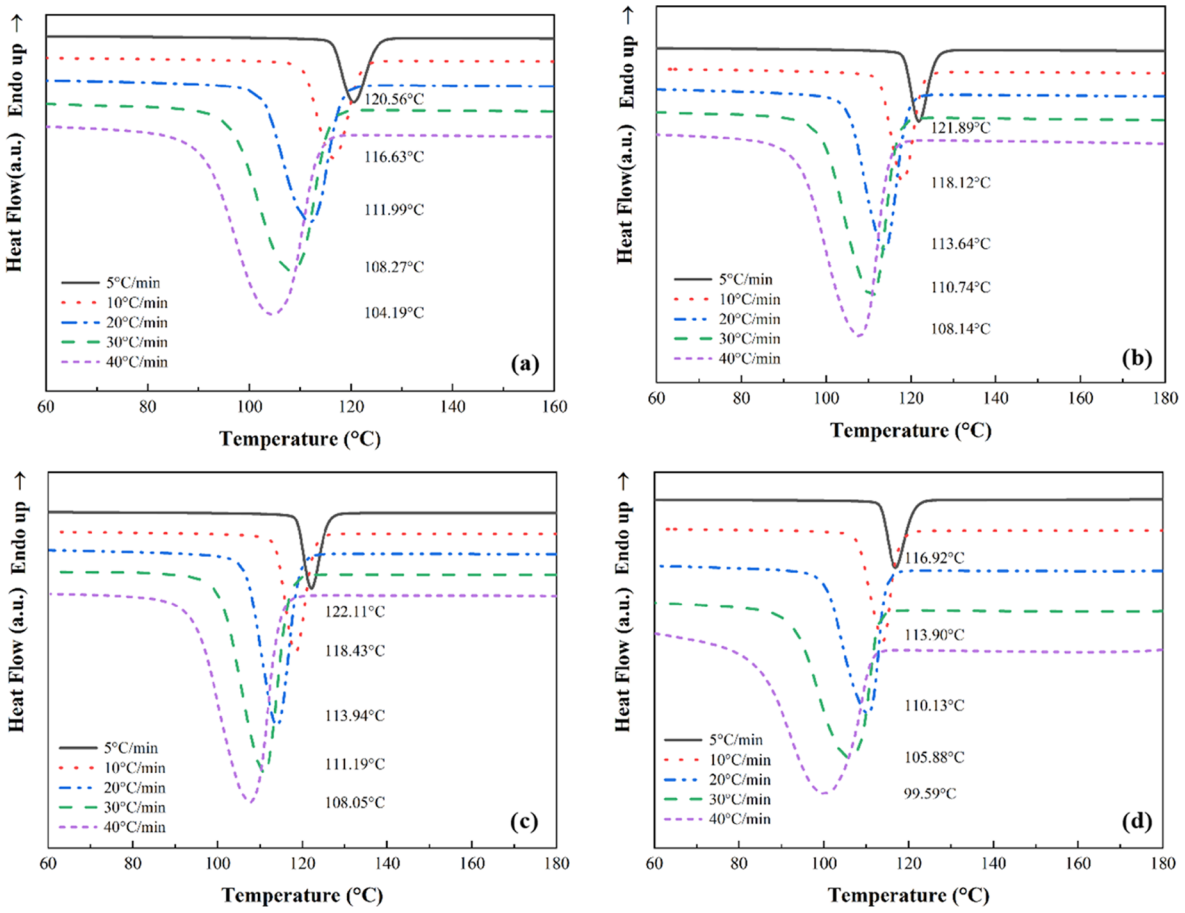

Figure 5. Cooling curves of (a) neat PP, (b) PP + 0.25% $Ti_3C_2T_x$, (c) PP + 0.5% $Ti_3C_2T_x$, and (d) PP + 1% $Ti_3C_2T_x$.

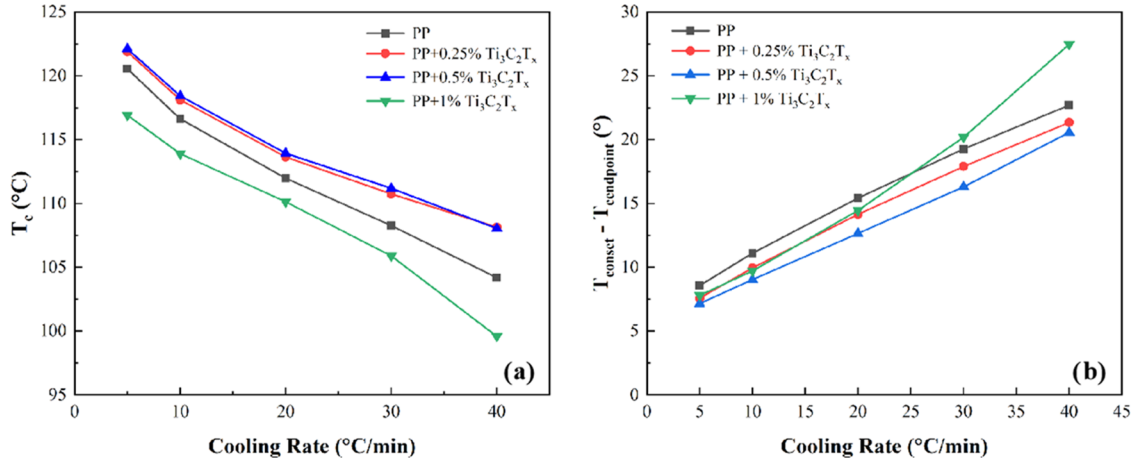

Figure 6. (a) Crystallization peak temperature (T_c) and (b) crystallization peak width ($T_{conset}-T_{cendpoint}$) of four samples.

The Avrami equation is often used to describe the isothermal crystallization kinetics by eq 2

$$X(t) = 1 - \exp(-kt^n) \quad (2)$$

where $X(t)$ is the relative crystallinity, t is the crystallization time, k is the crystallization rate constant, and n is the named Avrami exponent of which the value varies between 1 and 4 depending on the mechanism of nucleation and growth.[29] This equation can be expressed in the following form

$$\ln[-(1 - X_t)] = n \ln t + \ln k \quad (3)$$

Since the Avrami equation describes the crystallization process under constant temperature, the Jeziorny model[30] was applied to account for the nonisothermal crystallization condition.[31,32] In the Jeziorny model, the parameter k is modified by introducing the cooling rate ⌀, as in the following equation

$$\ln k_c = (\ln k)/\varnothing \quad (4)$$

The crystallization activation energy E_c is calculated from the plot of the crystallization peak temperature (T_c) and cooling rate (D) through the Kissinger method,[33−35] as shown in eq 5

https://doi.org/10.1021/acsomega.1c02970
ACS Omega 2021, 6, 19973−19982

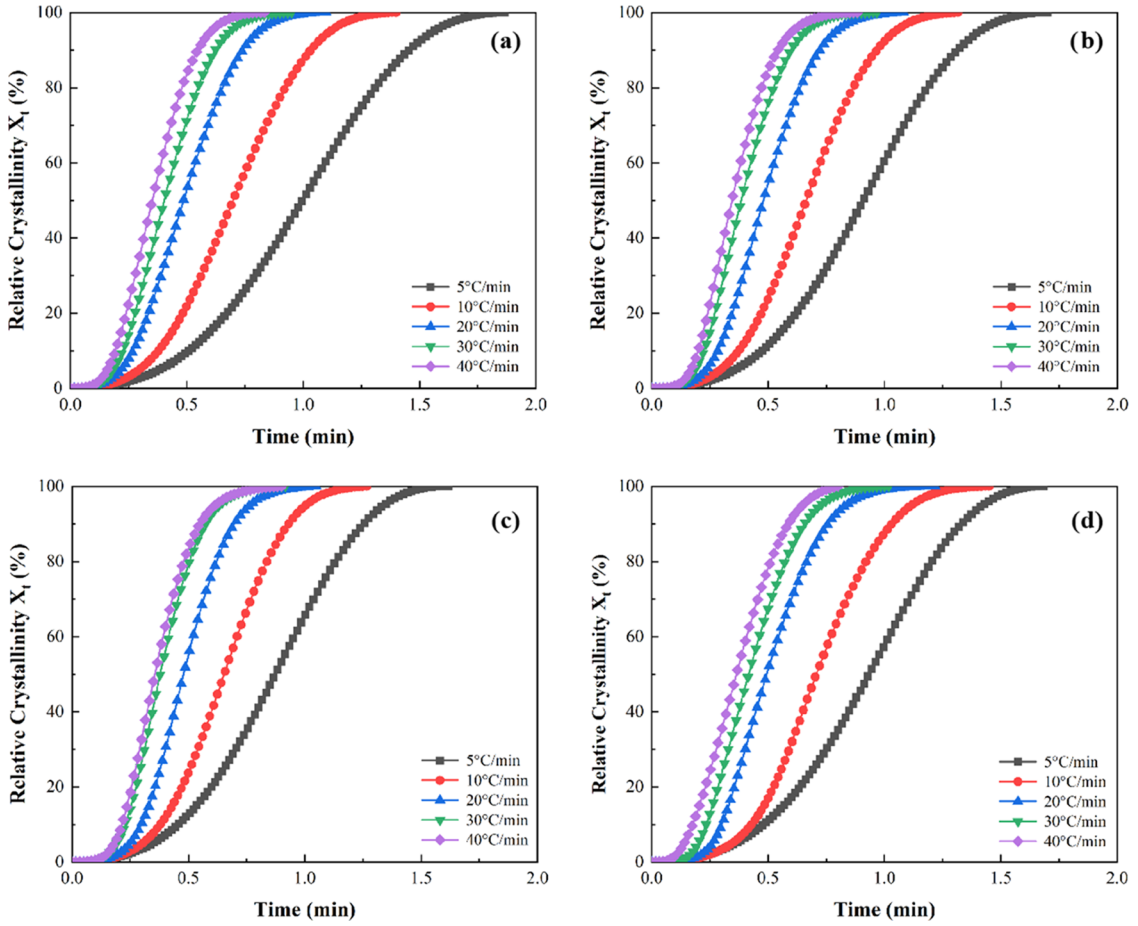

Figure 7. Plots of relative crystallinity as a function of time of (a) neat PP, (b) PP + 0.25% $Ti_3C_2T_x$, (c) PP + 0.5% $Ti_3C_2T_x$, and (d) PP + 1% $Ti_3C_2T_x$ at different cooling rates.

Table 1. Half-Crystallization Time $t_{1/2}$ of Four Samples

	$t_{1/2}$ (min)				
sample	5 °C/min	10 °C/min	20 °C/min	30 °C/min	40 °C/min
neat PP	1.00	0.70	0.49	0.40	0.35
PP + 0. 25% $Ti_3C_2T_x$	0.91	0.66	0.48	0.38	0.34
PP + 0. 5% $Ti_3C_2T_x$	0.87	0.65	0.48	0.38	0.36
PP + 1% $Ti_3C_2T_x$	0.93	0.71	0.49	0.42	0.36

$$\frac{\mathrm{d}[\ln(D/T_c^2)]}{\mathrm{d}\left(\frac{1}{T_c}\right)} = -\frac{E_c}{R} \tag{5}$$

where R is the universal gas constant, D is the cooling rate, and E_c is the activation energy. By integration, the equation can be expressed as

$$\ln\left(\frac{D}{T_c^2}\right) = \frac{1}{T_c}\left(-\frac{E_c}{R}\right) \tag{6}$$

From eq 6, the graph of $\ln(D/T_c^2)$ vs $(1/T_c)$ can be plotted and thereby the slope $(-E_c/R)$ and activation energy can be calculated. The Kissinger plot of the four samples is shown in Figure 8; the activation energy of the four samples follows the order: PP + 0.5% $Ti_3C_2T_xTi_3C_2T_x$ > PP + 0.25% $Ti_3C_2T_x$ > PP > PP + 1% $Ti_3C_2T_x$.

Table 2 indicates that the value of $\ln(k_c)$ first increases then decreases with a continuous increase in the fraction of

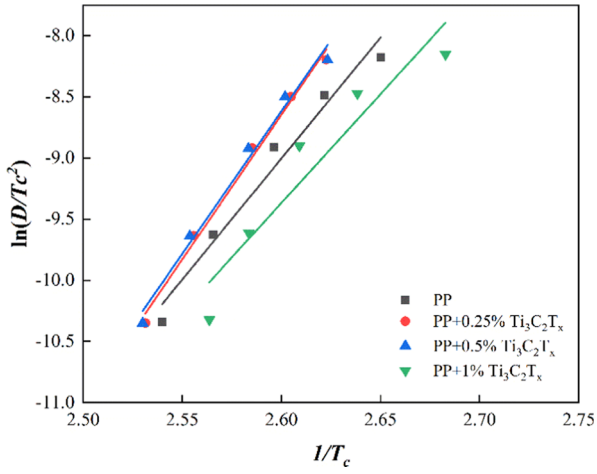

Figure 8. Plots of $\ln(D/T_c^2)$ versus $1/T_c$ of the four samples to calculate the activation energy E_c by the Kissinger method.

https://doi.org/10.1021/acsomega.1c02970
ACS Omega 2021, 6, 19973−19982

Table 2. Crystallization Kinetics Parameters of Four Samples

sample	E_c (kJ/mol)	cooling rate (°/min)	N	ln(k)	ln(k_c)
neat PP	−164.5	5	2.6	−0.24	−0.05
		10	2.8	0.67	0.07
		20	2.9	1.67	0.08
		30	3.0	1.68	0.06
		40	3.0	2.62	0.07
PP + 0.25% $Ti_3C_2T_x$	−196.5	5	2.6	0.03	0.01
		10	2.9	0.83	0.08
		20	3.1	1.76	0.09
		30	3.1	2.38	0.08
		40	3.1	2.69	0.07
PP + 0. 5% $Ti_3C_2T_x$	−193.8	5	2.6	0.11	0.02
		10	2.9	0.90	0.09
		20	3.2	1.88	0.09
		30	3.2	2.47	0.08
		40	3.2	2.68	0.07
PP + 1% $Ti_3C_2T_x$	−148.0	5	2.6	−0.03	−0.01
		10	3.0	0.61	0.06
		20	3.2	1.63	0.08
		30	3.2	2.20	0.07
		40	2.8	2.44	0.06

$Ti_3C_2T_x$. Since the value of ln(k_c) is related to the bulk crystallization rate, the results suggest that the crystallization rate would start to decrease once $Ti_3C_2T_x$ is added over a certain limit. It is known that the larger the activation energy, the more difficult the motion of polymer chains and thus greater the energy required to release during the crystallization process.[36] The activation energies of PP, PP + 0.25% $Ti_3C_2T_x$, PP + 0.5% $Ti_3C_2T_x$, and PP + 1% $Ti_3C_2T_x$ are −164.5, −196.5, −193.8, and −148.0 kJ/mol, respectively. The variation tendency of the activation energy is the same as that of the crystallization rate and the crystallization temperature. The crystallization parameters including the crystallization peak temperature, half-crystallization time, and nonisothermal crystallization kinetic constant suggest that with the addition of $Ti_3C_2T_x$, the crystallization process is accelerated during which $Ti_3C_2T_x$ might act as heterogeneous nuclei while the energy barrier is lowered. With the further addition of $Ti_3C_2T_x$, a rigid framework might be formed and impose a strong restrain on the crystal growth.[37] Therefore, at higher concentrations of $Ti_3C_2T_x$, the crystallization process would be surpassed, the crystallization parameters including the crystallization peak temperature and crystallization rate tend to shift to lower values.

2.3. Melting Behavior. Figure 9 displays the melting curves of the four samples. The heating rate is 10 °C/min, and the rate labeled above each curve means the cooling rate of the previous cooling cycle. The relative degree of crystallinity X_c can be determined from the melting curve by the following equation[38]

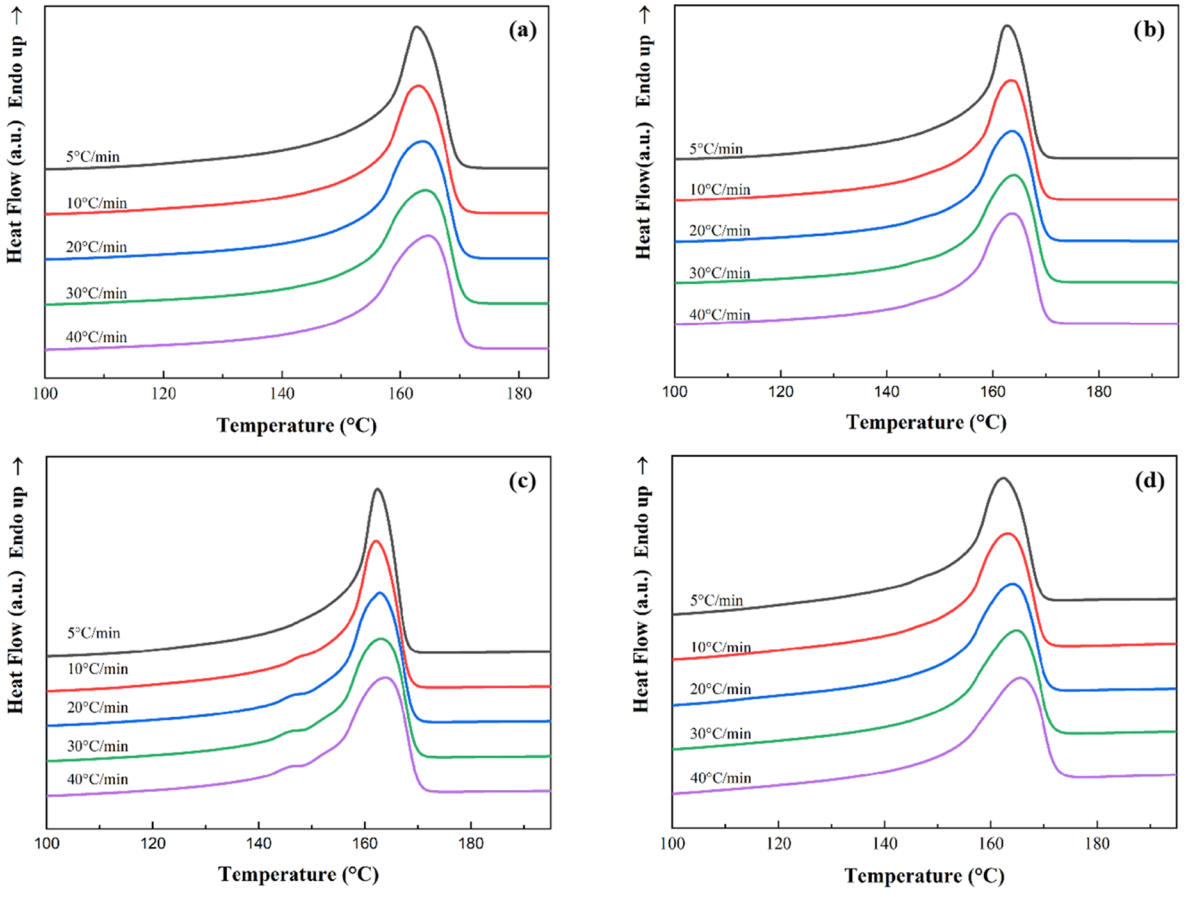

Figure 9. Melting curves of (a) neat PP, (b) PP + 0.25% $Ti_3C_2T_x$, (c) PP + 0.5% $Ti_3C_2T_x$, and (d) PP + 1% $Ti_3C_2T_x$ after the previous cooling cycle. The rate labeled above each curve is the cooling rate of the previous cooling cycle.

https://doi.org/10.1021/acsomega.1c02970
ACS Omega 2021, 6, 19973−19982

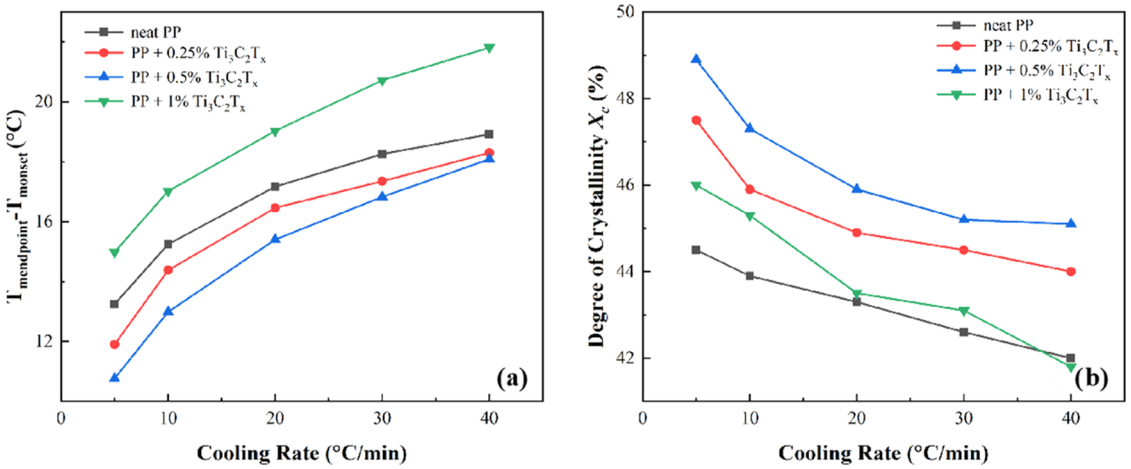

Figure 10. (a) Melting peak width ($T_{mendpoint}-T_{monset}$) and (b) degree of crystallinity (X_c) of four samples.

Table 3. Melting Parameters Four Samples

cooling rate (°C/min)	parameter (°C)	neat PP	PP + 0.25% $Ti_3C_2T_x$	PP + 0.5% $Ti_3C_2T_x$	PP + 1% $Ti_3C_2T_x$
5	T_m	162.7	162.8	162.4	162.5
	X_c (%)	44.5	47.5	48.9	46.0
10	T_m	163.1	163.4	162.1	163.1
	X_c (%)	43.9	45.9	47.3	45.3
20	T_m	163.8	163.8	162.8	164.2
	X_c (%)	43.3	44.9	45.9	43.5
30	T_m	164.3	164.1	163.0	164.8
	X_c (%)	42.6	44.5	45.2	43.1
40	T_m	164.7	164.3	163.8	165.5
	X_c (%)	42.0	44.0	45.1	41.8

$$X_c = \frac{\Delta H_m}{(1-x)\Delta H_0} \times 100\% \quad (7)$$

where ΔH_m is the enthalpy of melting, ΔH_0 is the enthalpy of melting when the material is 100% crystalline, which is 209 J g^{-1} for iPP in this case, and x is the weight fraction of $Ti_3C_2T_x$ in the sample.[39] It can be seen from Figure 9 that the change in melting peak temperature T_m is less obvious compared with crystallization peak temperature T_c. When the weight fraction of $Ti_3C_2T_x$ increases, the melting peak width first declines and then increases. Figure 10 and Table 3 indicate that both the melting peak width and the relative degree of crystallinity of the samples follow the order: PP + 0.5% $Ti_3C_2T_x$ > PP + 0.25% $Ti_3C_2T_x$ > PP > PP + 1% $Ti_3C_2T_x$. Similar to crystallization rate and activation energy, the crystallinity of $Ti_3C_2T_x$/PP composite starts to decline when the weight fraction of $Ti_3C_2T_x$ is 1%. This may arise from the aggregation of $Ti_3C_2T_x$, which restricts the chain movement and hinders the packing of polymer chains.

2.4. Wide-Angle X-ray Diffraction (WAXD) Characterization. PP is a semicrystalline polymer consisting of crystalline and amorphous phases. It is well-known that polypropylene has four crystalline forms α, β, γ, and mesomorphic depending on the arrangement and packing of chains.[40−42] Among them, the α form is most stable and commonly found in polypropylene; β form is metastable but has a higher toughness. To investigate the crystallite form in $Ti_3C_2T_x$/PP composites, WAXD was conducted since each form has a unique diffraction pattern.

Apart from the diffraction angle 2θ and lattice spacing, the crystallite dimension can also be calculated from the WAXD data by Debye−Scherrer's equation

$$L = k\lambda/\beta \cos(\theta) \quad (8)$$

where k is the shape factor and the value is taken as 0.9, L is the crystallite dimension, β is the diffraction line width at half maximum (FWHM) intensity in radians, and θ is the diffraction angle at the maximum peak.

The WAXD patterns and data are displayed in Figure 11 and Table 4. There are mainly five peaks at around 13.9, 16.9, 18.6, 21.1, and 21.8°, which correspond to $\alpha(110)$, $\alpha(040)$, $\alpha(130)$, $\alpha(111)$, and $\alpha(041)$, respectively. The distribution of the peaks proves that only α-form exists in the composites. Therefore, the addition of $Ti_3C_2T_x$ leads to the formation of the α-crystal phase, and the same result was also observed in the work of Shi et al.[22] It was found that the crystallinities of PP, PP + 0.25% $Ti_3C_2T_x$, PP + 0.5% $Ti_3C_2T_x$, and PP + 1% $Ti_3C_2T_x$ are 50.40, 52.80, 54.70, and 49.72% respectively, obtained from the WAXD results. The variation tendency of the crystallinity calculated from DSC and WAXD is consistent. From Table 4 it can be known that the addition of $Ti_3C_2T_x$ leads to a decrease in crystallite size. The sample that contains 0.5 wt % $Ti_3C_2T_x$ has the smallest crystallite size.

3. CONCLUSIONS

In this work, $Ti_3C_2T_x$, a typical member of 2D MXenes was successfully fabricated by etching. Then, different weight fractions of $Ti_3C_2T_x$ were mixed with PP by melt blending to study the nonisothermal crystallization kinetics of the resulting

https://doi.org/10.1021/acsomega.1c02970
ACS Omega 2021, 6, 19973−19982

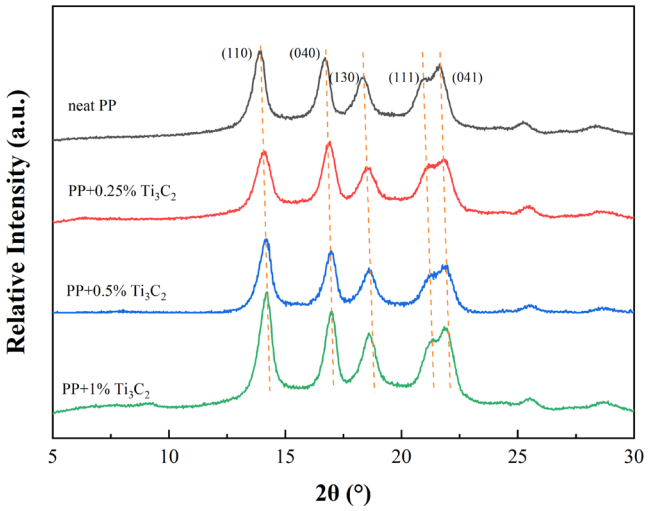

Figure 11. WAXD patterns of four samples prepared under the same conditions.

composites. When the amount of $Ti_3C_2T_x$ added is increased from 0 to 0.5 wt %, the crystallization peak temperature and crystallization rate both increase, indicating that the crystallization process is promoted. Once the weight percentage of $Ti_3C_2T_x$ reaches 1 wt %, the crystallization process requires larger supercooling, and the crystallization rate drops. The calculated activation energy is −164.5, −196.5, −193.8, and −147.95 kJ/mol, showing the same variation tendency as that of the crystallization peak temperature and rate. The WAXD results reveal that the crystallite size of nanocomposite with 0.5 wt % $Ti_3C_2T_x$ is the smallest. Moreover, only α-form crystallite exists in the composites; therefore, it can be concluded that $Ti_3C_2T_x$ acts as an α-form nucleating agent in the crystallization process.

4. EXPERIMENTAL

4.1. Materials. The Ti_3AlC_2 powders with 99% purity (400 mesh) were purchased from 11 Technology Co. Ltd., China. Lithium fluoride (LiF, 99% purity) was purchased from Aladdin Bio-Chem Technology Co. Ltd., China. Concentrated hydrochloric acid (HCl, 37 wt %) was purchased from Chengdu Kelong Chemical Reagent Factory, China. The isotactic polypropylene resin (trade name T38F) was obtained from Lanzhou PetroChemical Corp., China. The weighted-average molecular weight M_w is 347 200 g/mol and average isotacticity tested by high-temperature solution ^{13}C NMR is 97%.

4.2. Sample Preparation. *4.2.1. Etching of Ti_3AlC_2.* In this work, the MAX phase Ti_3AlC_2 was etched by in situ HF formation. First, 19.5 mL of concentrated HCl was added to 20 mL of distilled water. LiF powders (2.5 g) were added to the diluted HCl under magnetic stirring. Then, 2.5 g of Ti_3AlC_2 powders was slowly added to the solution within 10 min to avoid overheating caused by the exothermic reaction. The mixture was held at 40 °C for 24 h under continuous stirring. When the etching was completed, the resulting mixture was purified by washing with distilled water and centrifuging at 8000 rpm for 10 min. This washing−centrifugation cycle was repeated until the supernatant reached a pH value of around 6.

Then, the sediment was added with distilled water, followed by ultrasonication in an ice-bath for 2 h and centrifugation. Finally, the supernatant was collected and dried under a vacuum.

4.2.2. Preparation of Ti_3C_2/iPP Composites. In the first step, the $Ti_3C_2T_x$ powder was mixed with PP granules to obtain the $Ti_3C_2T_x$/iPP masterbatch with a $Ti_3C_2T_x$ concentration of 2.5 wt %. During the melt mixing process, a Brabender internal mixer with a 50 cm^3 mixing chamber was used. The polypropylene granules and $Ti_3C_2T_x$ were first slowly added to the internal mixer under a temperature of 190 °C and a rotation speed of 10 rpm and kept for 10 min. After that, the rotation speed was set to 50 rpm for 7 min. Then, the $Ti_3C_2T_x$/PP masterbatch, $Ti_3C_2T_x$ powder, and PP granules were mixed again in the internal mixer under the same conditions to prepare samples with different $Ti_3C_2T_x$ weight percentages (0, 0.25, 0.5, and 1 wt %). After that, the mixture was compressed by a pressure molding machine at 8 MPa and 190 °C for further characterization.

4.3. Characterization. *4.3.1. Differential Scanning Calorimetry (DSC).* All nonisothermal crystallization experiments were performed with Mettler Toledo DSC3 (Mettler, Switzerland) differential scanning calorimetry under a continuous nitrogen flow of 50 mL/min. The standard procedure for each experiment was as follows: 4−5 mg of the sample was weighed, heated to 200 °C at a rate of 10 °C/min, and held for 5 min to eliminate previous thermal history.[43−46] Then, the sample was cooled to 50 °C at different cooling rates, i.e., 5, 10, 20, 30, and 40 °C/min, to analyze the crystallization behavior. After cooling, the sample was heated

Table 4. WAXD Data of Four Samples

		(*hkl*)				
parameters	sample	(110)	(040)	(130)	(111)	(041)
2θ (deg)	neat PP	13.9	16.7	18.3	20.9	21.7
	PP + 0.25% $Ti_3C_2T_x$	14.1	16.9	18.5	21.2	21.8
	PP + 0.5% $Ti_3C_2T_x$	14.2	17.0	18.6	21.1	21.9
	PP + 1% $Ti_3C_2T_x$	14.2	17.0	18.6	21.1	21.9
d-spacing (Å)	neat PP	6.4	5.3	4.8	4.2	4.1
	PP + 0.25% $Ti_3C_2T_x$	6.3	5.2	4.8	4.2	4.1
	PP + 0.5% $Ti_3C_2T_x$	6.2	5.2	4.8	4.2	4.0
	PP + 1% $Ti_3C_2T_x$	6.2	5.2	4.8	4.2	4.1
L (nm)	neat PP	13.1	14.8	12.1	12.6	8.4
	PP + 0.25% $Ti_3C_2T_x$	11.0	12.6	9.4	8.2	9.9
	PP + 0.5% $Ti_3C_2T_x$	13.0	14.3	10.9	10.2	8.3
	PP + 1% $Ti_3C_2T_x$	12.7	14.3	10.8	16.6	10.1

https://doi.org/10.1021/acsomega.1c02970
ACS Omega 2021, 6, 19973−19982

from 50 to 200 °C at a rate of 10 °C/min to analyze the melting behavior.

The relative crystallinity (X_t) of the sample at a given crystallization time (t) could be calculated using the following equation

$$X_t = \int_0^t (dH/dt)dt / \int_0^\infty (dH/dt)/dt \quad (9)$$

The half time of crystallization ($t_{1/2}$) can be calculated from the curve when the relative crystallinity is 50% and can be used to evaluate the crystallization rate. At an identical cooling rate, a lower crystallization half time indicates a higher overall crystallization rate.

4.3.2. X-ray Diffraction (XRD). The XRD patterns of Ti_3AlC_2, $Ti_3C_2T_x$, and $Ti_3C_2T_x$/PP composites were obtained through a diffractor (Ultima IV, Rigaku, Japan). The wavelength of Cu Kα radiation was λ = 0.154 nm and the scanning rate was 2°/min. For Ti_3AlC_2 and $Ti_3C_2T_x$, powder samples were used and spectra were recorded in the range of 2θ = 2−80°. Wide-angle X-ray diffraction (WAXD) was applied for $Ti_3C_2T_x$/PP composites; the samples were first hot molded into 1 mm thick sheets before taking the measurements. The scanning range was 2θ = 5−40°.

4.3.3. Scanning Electron Microscopy (SEM) and Energy-Dispersive Spectroscopy (EDS). The morphologies and composition of precursor Ti_3AlC_2 and $Ti_3C_2T_x$ particles were observed via scanning electron microscopy (SEM, Apreo S HiVoc, Thermo Fisher Scientific) equipped with energy-dispersive spectroscopy (EDS).

4.3.4. Transmission Electron Microscopy (TEM). To further analyze the structure of $Ti_3C_2T_x$, TEM (Tecnai G2 F20 S-TWIN, FEI) was performed under an accelerating voltage of 200 kV. The TEM sample was prepared by dispersion in distilled water and under ultrasonication for 30 min; then, the dispersion was dropped on the copper grid for further observation.

AUTHOR INFORMATION

Corresponding Authors

Jian Kang − *State Key Laboratory of Polymer Materials Engineering, Polymer Research Institute of Sichuan University, 610065 Chengdu, China;* orcid.org/0000-0002-3888-2462; Email: jiankang@scu.edu.cn

Jingping Li − *Office of Scientific Research Development, Sichuan University, 610065 Chengdu, China;* Email: jingpingli@scu.edu.cn

Authors

Wanxin Peng − *State Key Laboratory of Polymer Materials Engineering, Polymer Research Institute of Sichuan University, 610065 Chengdu, China*

Ran Hu − *State Key Laboratory of Polymer Materials Engineering, Polymer Research Institute of Sichuan University, 610065 Chengdu, China*

Weijiao Jiang − *State Key Laboratory of Polymer Materials Engineering, Polymer Research Institute of Sichuan University, 610065 Chengdu, China*

Ya Cao − *State Key Laboratory of Polymer Materials Engineering, Polymer Research Institute of Sichuan University, 610065 Chengdu, China*

Ming Xiang − *State Key Laboratory of Polymer Materials Engineering, Polymer Research Institute of Sichuan University, 610065 Chengdu, China*

Complete contact information is available at: https://pubs.acs.org/10.1021/acsomega.1c02970

Notes

The authors declare no competing financial interest.

ACKNOWLEDGMENTS

This work was support by the Fundamental Research Funds for the Central Universities, the National Natural Science Foundation of China (NSFC, Grant nos. 51503134 and 51702282), and State Key Laboratory of Polymer Materials Engineering (Grant no. SKLPME 2017-3-02).

REFERENCES

(1) Novoselov, K. S.; Geim, A. K.; Morozov, S. V.; Jiang, D.; Zhang, Y.; Dubonos, S. V.; Grigorieva, I. V.; Firsov, A. A. Electric field effect in atomically thin carbon films. *Science* **2004**, *306*, 666−9.

(2) Peng, Y.; Li, Y.; Ban, Y.; Jin, H.; Jiao, W.; Liu, X.; Yang, W. Metal-organic framework nanosheets as building blocks for molecular sieving membranes. *Science* **2014**, *346*, 1356−1359.

(3) Rodenas, T.; Luz, I.; Prieto, G.; Seoane, B.; Miro, H.; Corma, A.; Kapteijn, F.; Xamena, F. X. L. I.; Gascon, J. Metal-organic framework nanosheets in polymer composite materials for gas separation. *Nat. Mater* **2015**, *14*, 48.

(4) Colson, J. W.; Woll, A. R.; Mukherjee, A.; Levendorf, M. P.; Spitler, E. L.; Shields, V. B.; Spencer, M. G.; Park, J.; Dichtel, W. R. Oriented 2D covalent organic framework thin films on single-layer graphene. *Science* **2011**, *332*, 228−31.

(5) Liu, H.; Du, Y.; Deng, Y.; Ye, P. D. Semiconducting black phosphorus: synthesis, transport properties and electronic applications. *Chem. Soc. Rev.* **2015**, *44*, 2732−43.

(6) Zhang; Hua. Ultrathin Two-Dimensional Nanomaterials. *ACS Nano* **2015**, *9*, 9451−69.

(7) Naguib, M.; Kurtoglu, M.; Presser, V.; Lu, J.; Niu, J.; Heon, M.; Hultman, L.; Gogotsi, Y.; Barsoum, M. W. Two-dimensional nanocrystals produced by exfoliation of Ti3 AlC2. *Adv. Mater.* **2011**, *23*, 4248−53.

(8) Jimmy, J.; Kandasubramanian, B. Mxene functionalized polymer composites: Synthesis and applications. *Eur. Polym. J.* **2020**, *122*, No. 109367.

(9) Verger, L.; Xu, C.; Natu, V.; Cheng, H.-M.; Ren, W.; Barsoum, M. W. Overview of the synthesis of MXenes and other ultrathin 2D transition metal carbides and nitrides. *Curr. Opin. Solid State Mater. Sci.* **2019**, *23*, 149−163.

(10) Spector, M.; Ang, A. S.; Minin, O. V.; Minin, I. V.; Karabchevsky, A. Photonic hook formation in near-infrared with MXene Ti3C2 nanoparticles. *Nanoscale Adv.* **2020**, *2*, 5312−5318.

(11) Zhang, H.; Wang, L.; Chen, Q.; Li, P.; Zhou, A.; Cao, X.; Hu, Q. Preparation, mechanical and anti-friction performance of MXene/polymer composites. *Mater. Des.* **2016**, *92*, 682−689.

(12) Woo, J. H.; Kim, N. H.; Kim, S. I.; Park, O.-K.; Lee, J. H. Effects of the addition of boric acid on the physical properties of MXene/polyvinyl alcohol (PVA) nanocomposite. *Composites, Part B* **2020**, *199*, No. 108205.

(13) Liu, C.; Wu, W.; Shi, Y.; Yang, F.; Liu, M.; Chen, Z.; Yu, B.; Feng, Y. Creating MXene/reduced graphene oxide hybrid towards highly fire safe thermoplastic polyurethane nanocomposites. *Composites, Part B* **2020**, *203*, No. 108486.

(14) Shi, Y.; Liu, C.; Duan, Z.; Yu, B.; Liu, M.; Song, P. Interface engineering of MXene towards super-tough and strong polymer nanocomposites with high ductility and excellent fire safety. *Chem. Eng. J.* **2020**, *399*, No. 125829.

(15) Esthappan, S. K.; Kuttappan, S. K.; Joseph, R. Effect of titanium dioxide on the thermal ageing of polypropylene. *Polym. Degrad. Stab.* **2012**, *97*, 615−620.

(16) Kang, J.; Cao, Y.; Li, H.; Li, J.; Chen, S.; Yang, F.; Xiang, M. Influence of the stereo-defect distribution on the crystallization

behavior of Ziegler-Natta isotactic polypropylene. *J. Polym. Res.* **2012**, *19*, No. 1708.
(17) Wu, K.; Zhao, Y.; Li, J.; Yao, J.; Chen, X.; Shao, Z. Crystallization, Mechanical, and Antimicrobial Properties of Diallyl Cyanuric Derivative-Grafted Polypropylene. *ACS Omega* **2021**, *6*, 12794−12800.
(18) Yang, H.; Zhang, X.; Qu, C.; Li, B.; Zhang, L.; Zhang, Q.; Fu, Q. Largely improved toughness of PP/EPDM blends by adding nano-SiO2 particles. *Polymer* **2007**, *48*, 860−869.
(19) Chen, Y.; Yin, Q.; Zhang, X.; Xue, X.; Jia, H. The crystallization behaviors and rheological properties of polypropylene/graphene nanocomposites: The role of surface structure of reduced graphene oxide. *Thermochim. Acta* **2018**, *661*, 124−136.
(20) Chen, J.; Li, X.; Wu, C. Crystallization Behavior of Polypropylene Filled with Modified Carbon Black. *Polym. J* **2007**, *39*, 722−730.
(21) Chen, M.; Tian, G.; Zhang, Y.; Wan, C.; Zhang, Y. Effect of silicon dioxide on crystallization and melting behavior of polypropylene. *J. Appl. Polym. Sci.* **2006**, *100*, 1889−1898.
(22) Shi, Y.; Liu, C.; Liu, L.; Fu, L.; Yu, B.; Lv, Y.; Yang, F.; Song, P. Strengthening, toughing and thermally stable ultra-thin MXene nanosheets/polypropylene nanocomposites via nanoconfinement. *Chem. Eng. J.* **2019**, *378*, No. 122267.
(23) Wang, K.; Zhou, Y.; Xu, W.; Huang, D.; Wang, Z.; Hong, M. Fabrication and thermal stability of two-dimensional carbide Ti3C2 nanosheets. *Ceram. Int.* **2016**, *42*, 8419−8424.
(24) Liu, R.; Li, W. High-Thermal-Stability and High-Thermal-Conductivity Ti3C2T x MXene/Poly(vinyl alcohol) (PVA) Composites. *ACS Omega* **2018**, *3*, 2609−2617.
(25) Alhabeb, M.; Maleski, K.; Anasori, B.; Lelyukh, P.; Clark, L.; Sin, S.; Gogotsi, Y. Guidelines for Synthesis and Processing of Two-Dimensional Titanium Carbide (Ti3C2Tx MXene). *Chem. Mater.* **2017**, *29*, 7633−7644.
(26) Munir, S.; Rasheed, A.; Rasheed, T.; Ayman, I.; Ajmal, S.; Rehman, A.; Shakir, I.; Agboola, P. O.; Warsi, M. F. Exploring the Influence of Critical Parameters for the Effective Synthesis of High-Quality 2D MXene. *ACS Omega* **2020**, *5*, 26845−26854.
(27) Scheibe, B.; Kupka, V.; Peplinska, B.; Jarek, M.; Tadyszak, K. The Influence of Oxygen Concentration during MAX Phases (Ti(3)AlC(2)) Preparation on the alpha-Al(2)O(3) Microparticles Content and Specific Surface Area of Multilayered MXenes (Ti(3)C(2)Tx). *Materials* **2019**, *12*, No. 353.
(28) Cao, X.; Wu, M.; Zhou, A.; Wang, Y.; He, X.; Wang, L. Non-isothermal crystallization and thermal degradation kinetics of MXene/linear low-density polyethylene nanocomposites. *e-Polymers* **2017**, *17*, 373−381.
(29) Avrami, M. Kinetics of Phase Change. I General Theory. *J. Chem. Phys.* **1939**, *7*, 1103−1112.
(30) Jeziorny, A. Parameters characterizing the kinetics of the non-isothermal crystallization of poly(ethylene terephthalate) determined by d.s.c. *Polymer* **1978**, *19*, 1142−1144.
(31) Layachi, A.; Makhlouf, A.; Frihi, D.; Satha, H.; Belaadi, A.; Seguela, R. Non-isothermal crystallization kinetics and nucleation behavior of isotactic polypropylene composites with micro-talc. *J. Therm. Anal. Calorim.* **2019**, *138*, 1081−1095.
(32) Coburn, N.; Douglas, P.; Kaya, D.; Gupta, J.; McNally, T. Isothermal and non-isothermal crystallization kinetics of composites of poly(propylene) and MWCNTs. *Adv. Ind. Eng. Polym. Res.* **2018**, *1*, 99−110.
(33) Wei, Z.; Zhang, W.; Chen, G.; Liang, J.; Shu, Y.; Pei, W.; Lian, L. Crystallization and melting behavior of isotactic polypropylene nucleated with individual and compound nucleating agents. *J. Therm. Anal. Calorim.* **2010**, *102*, 775−783.
(34) Ariffin, A.; Ariff, Z. M.; Jikan, S. S. Evaluation on nonisothermal crystallization kinetics of polypropylene/kaolin composites by employing Dobreva and Kissinger methods. *J. Therm. Anal. Calorim.* **2011**, *103*, 171−177.
(35) Hao, W.; Li, W.; Wen, Y.; Shen, L. Effect of silicon nitride nanoparticles on the crystallization behavior of polypropylene. *Polym. Test.* **2011**, *30*, 527−533.
(36) Şanlı, S.; Durmus, A.; Ercan, N. Isothermal crystallization kinetics of glass fiber and mineral-filled polyamide 6 composites. *J. Mater. Sci.* **2012**, *47*, 3052−3063.
(37) Huang, Z.; Wang, S.; Kota, S.; Pan, Q.; Barsoum, M. W.; Li, C. Y. Structure and crystallization behavior of poly(ethylene oxide)/Ti3C2Tx MXene nanocomposites. *Polymer* **2016**, *102*, 119−126.
(38) El Achaby, M.; Arrakhiz, F.-E.; Vaudreuil, S.; el Kacem Qaiss, A.; Bousmina, M.; Fassi-Fehri, O. Mechanical, thermal, and rheological properties of graphene-based polypropylene nanocomposites prepared by melt mixing. *Polym. Compos.* **2012**, *33*, 733−744.
(39) Jiang, W.; Song, Y.; Song, X.; Zhang, Y.; Xiang, M. Influences of Molecular Structure on the Non-Isothermal Crystallization Behavior of β-Nucleated Isotactic Polypropylene. *Polym. Sci., Ser. A* **2020**, *62*, 616−629.
(40) Keith, H. D.; Padden, F. J.; Walter, N. M.; Wyckoff, H. W. Evidence for a Second Crystal Form of Polypropylene. *J. Appl. Phys.* **1959**, *30*, 1485−1488.
(41) Dimeska, A.; Phillips, P. J. High pressure crystallization of random propylene−ethylene copolymers: $\alpha-\gamma$ Phase diagram. *Polymer* **2006**, *47*, 5445−5456.
(42) Mileva, D.; Androsch, R.; Zhuravlev, E.; Schick, C.; Wunderlich, B. Homogeneous nucleation and mesophase formation in glassy isotactic polypropylene. *Polymer* **2012**, *53*, 277−282.
(43) Qian, J.; He, P.; Nie, K. Nonisothermal crystallization of PP/nano-SiO2 composites. *J. Appl. Polym. Sci.* **2004**, *91*, 1013−1019.
(44) Tjong, S. C.; Shi, A. X. Non-isothermal crystallization kinetics of calcium carbonate-filled β-crystalline phase polypropylene composites. *Polym. Int.* **1997**, *44*, 95−103.
(45) Luo, J.; Liu, M.; Chen, J.; Min, J.; Fu, Q.; Zhang, J. Effectively maintaining the disentangled state of isotactic polypropylene in the presence of graphene nanoplatelet. *Polymer* **2021**, *226*, No. 123806.
(46) Harnisch, K.; Muschik, H. Determination of the Avrami exponent of partially crystallized polymers by DSC (DTA) analyses. *Colloid Polym. Sci.* **1983**, *261*, 908−913.

https://doi.org/10.1021/acsomega.1c02970
ACS Omega 2021, 6, 19973−19982